Journal of Power Sources 196 (2011) 4779–4784

Contents lists available at ScienceDirect

Journal of Power Sources

journal homepage: www.elsevier.com/locate/jpowsour

Synthesis and rate performance of Fe_3O_4-based Cu nanostructured electrodes for Li ion batteries

Huanan Duan[a,1], Joe Gnanaraj[b], Jianyu Liang[a,*]

[a] Department of Mechanical Engineering, Worcester Polytechnic Institute, 100 Institute Rd, Worcester, MA 01609, United States
[b] Yardney Technical Products, Inc., 82 Mechanic Street, Pawcatuck, CT 06379, United States

ARTICLE INFO

Article history:
Received 16 November 2010
Received in revised form
29 December 2010
Accepted 7 January 2011
Available online 19 January 2011

Keywords:
Nanostructured anode
Li ion battery
Template assisted electrodeposition
Morphology
Rate capability

ABSTRACT

Fe_3O_4-based Cu nanostructured electrodes for Li ion batteries are fabricated by a two-step electrochemical process, and characterized with scanning electron microscopy, X-ray diffraction, and electrochemical experiments. It is found that the electrochemical performance is closely related to the Fe_3O_4 morphology. The nanostructured electrodes with 1 min Fe_3O_4 deposition exhibit a large specific discharge capacity, i.e. 1342.23 mAh g^{-1} in the first cycle and 1003.94 mAh g^{-1} in the 34th. After extended Fe_3O_4 electroplating, Fe_3O_4 particles will fill the spaces between the Cu nanorods and coalesce on the top of the Cu nanorod arrays, which is detrimental to achieve high specific reversible capacities and good rate capability. Moreover, the nanostructured electrodes demonstrate significantly enhanced cycling performance due to the introduction of Cu nanorod arrays as the current collector, especially as compared to the planar electrodes where Fe_3O_4 is electrodeposited directly onto planar Cu surfaces.

1. Introduction

Lithium ion (Li ion) batteries are attractive candidates as a power source in hybrid and electric vehicles due to their high specific energy, large energy density and good cycle life. To this end, the development of electrodes with high specific capacity at high discharge/charge rate is a must, however is beyond the current Li ion technology [1–6]. Nanostructured materials have potential to satisfy this demand. They have many potential advantages including [7–9]: (1) short Li ion transport length due to small particle size; (2) higher charge/discharge rate as a result of increased electrode/electrolyte contact area; (3) better accommodation of the strain induced by structure change in active materials; and (4) short path lengths for electronic transport which may permit operation with low electronic conductivity at high power.

In recent years, many efforts have been dedicated to seeking superior anode materials. Among them includes the renewed interest of metal oxides, sulfides, and phosphides based on the so-called "conversion reaction", as expressed in Eq. (1) [10]

$$M_xX_y + ne^- + nLi^+ \leftrightarrow xM^0 + yLi_nX_y \quad (1)$$

where M is a transition metal. Such types of electrode materials typically reduce the overall cell voltage, but exhibit high specific capacity. In addition, due to the high potential against lithium, side reactions with the electrolyte are minimized. Fe_3O_4, for example, has a theoretical capacity of approximately 928 mAh g^{-1} by assuming the reduction of Fe^{3+} and Fe^{2+} to Fe^0 during Li ion intercalation, which is about three times that of commonly used graphitic carbons [11,12]. Other benefits of Fe_3O_4 include high relative electronic conductivity, cost-efficiency, and environmentally friendliness. As a result, nanostructured hematite and magnetite have attracted a lot of attention as candidate anode materials [1,7,10–14].

A typical process to incorporate nanostructured active materials into anodes is as following: the previously synthesized nanomaterials are mixed with conducting carbon black and polymer binder such as poly(vinyldifluoride) (PVDF). The materials are mixed at a specific weight ratio, and are pressed on various current collectors including Ni mesh or Cu foil to form working electrodes [11,13–15]. Cathodic electrodeposition is an alternative method to make nanostructured anodes. Herein active nanomaterials are deposited directly onto the current collector, and the material load is determined by the electrodeposition time [10,12,16]. This procedure has the potential to simplify the electrode fabrication process, address the issues of agglomeration and dispersion during mixing, guarantee an intimate contact between the active materials with the current collector, and enable good deposition control.

In this paper, we report our continuing effort to seek a non-toxic, nano-engineered electrode synthesized by a two-step fabrication

* Corresponding author. Tel.: +1 508 831 6649; fax: +1 508 831 5178.
E-mail address: jianyul@wpi.edu (J. Liang).
[1] Present address: Bard 214, Department of Materials Science and Engineering, Cornell University, Ithaca, NY 14850, United States.

0378-7753/$ – see front matter © 2011 Elsevier B.V. All rights reserved.
doi:10.1016/j.jpowsour.2011.01.029

process using a Fe_3O_4/Cu material system. Similar investigation in this system has been reported before [12] followed by only a couple of reported studies on similar material systems with limited success [16–18]. This might be due to the fact that control over the morphology of the active material is of critical importance in achieving the desired electrode performance even with the presence of the Cu nanorod arrays. We want to emphasize the importance of electrodeposition conditions, such as time and temperature, on obtaining the desired dense and crack-free morphology of Fe_3O_4. Only with the crystalline Fe_3O_4 nanoparticles deposited between Cu nanorods can good rate performance be obtained. Since the morphology of Fe_3O_4 deposited after prolonged deposition time in our study [19] is very different from previous reports [12] due to different deposition conditions used, comparison to both the nanostructured electrodes with longer deposition time and planar electrodes is reported in this paper, and the effect of morphology on the capacity retention on both nanostructured and planar electrodes is discussed. In addition, nanostructured electrodes with 1 min Fe_3O_4 deposition time under the optimized conditions demonstrated a high specific capacity of 1342.23 mAh g^{-1} during the initial discharge, which is the highest value ever reported; a brief discussion on the cause of this property is provided.

2. Experimental

2.1. Fabrication of Cu nanorod arrays as current collectors

The detailed description of the fabrication of Cu nanorod arrays as the current collector can be found in Ref. [16]. Briefly, Cu nanorod arrays were fabricated by AAO template-assisted (Whatman, Anodisc 13) cathodic electrodeposition using a two electrode configuration from an electrolytic solution containing 100 g L^{-1} $CuSO_4{\cdot}5H_2O$ (Alfa Aesar), 20 g L^{-1} $(NH_4)_2SO_4$ (Alfa Aesar), and 80 mL L^{-1} diethylenetriamine (DETA, Alfa Aesar). Two mechanically polished pieces of Cu disks (1.3 cm in diameter, from Yardney Technical Products, Inc.) served as the cathode and the anode. The electrochemical depositions were carried out at 1.2 DC V at room temperature for 5 min. After the electrodeposition, the AAO templates were dissolved in a 2 M NaOH solution. Finally, the surface oxides of the Cu nanorods were cleaned in a dilute HCl solution.

2.2. Electrodeposition of Fe_3O_4

Active material of Fe_3O_4 was deposited on the Cu disks with Cu nanorod arrays by electrodeposition. The electrolyte consisted of 2 M NaOH (Alfa Aesar) and 0.09 M $Fe_2(SO_4)_3{\cdot}5H_2O$ (Alfa Aesar) complexed with 0.1 M tri-ethanol-amine (Acros Organics) at a pH value of 12.3 [10,12,19,20]. Electrodeposition was carried out at a current density of -5 mA cm^{-2} and 80 °C. The Cu disks with Cu nanorods served as the cathode while a graphite sheet served as the anode. Fe_3O_4 was also electrodeposited under the same conditions on mechanically polished planar Cu disks to provide comparison samples.

2.3. Structure analysis and morphology characterization

The as-prepared nanostructured electrodes were examined by X-ray diffraction (XRD) using a REGAKU CN2182D5 diffractometer and by scanning electron microscopy (SEM) using a JEOL JSM-7000 microscope.

2.4. Electrochemical tests

The electrochemical performance of the nanostructured electrodes was evaluated on coin cells. Coin cells were constructed using metallic lithium as the counter electrodes and the nanostructured or planar electrodes as the anodes under argon atmosphere inside a glove box [16]. The coin cells were cycled galvanostatically between 2.5 and 0.02 V versus Li^+/Li^0 at different rates including $C/20$, $C/10$, $C/5$, and $C/2$, with C being defined as the full use of the capacity in 1 h. The charge/discharge capacities and the capacity retention property of the anodes at different charge/discharge current densities were recorded.

3. Results and discussion

3.1. Morphology of Fe_3O_4-based Cu nanostructured electrodes

The two-step fabrication process consists of electrodeposition of Cu nanorod arrays on mechanically polished planar Cu disks and electrodeposition of the active material of Fe_3O_4 onto the Cu nanorod arrays. Several benefits of introducing Cu nanorod arrays as the current collector include: (1) greatly increasing the surface area of the Cu disk, enabling high loading of active materials and large reaction area during Li ion intercalation/deintercalation; (2) providing an intimate contact with and mechanically strong support to the nanostructured Fe_3O_4 deposits; (3) inhibiting the agglomeration of Fe_3O_4 nanoparticles during charge/discharge cycles. SEM images in Fig. 1a and b depict the top and cross-sectional view of the Cu nanorod arrays deposited on mechanically polished Cu disks after removing the AAO template. Clearly, the morphology of the Cu nanorods duplicates that of the nanopores within the AAO template. The structures have diameters of 200 nm, are uniformly distributed, and perpendicular to the Cu substrate [21–23]. The cross-sectional view in Fig. 1b suggests that approximately 1600 nm long Cu nanorods can be obtained after 5 min of Cu electrodeposition. By varying the electrodeposition duration and utilizing different AAO templates with varying pore sizes and pore density, we are able to control the length, diameter, and inter-rod distance of the electrodeposited Cu nanaorods [12,16], which is favorable to control the load of the active materials. However, there is a compromise between the length and diameter of Cu nanorods. We have found that the aspect ratio of the Cu nanorods cannot be too large to obtain free-standing Cu nanorod arrays without aggregation and avoid blocking the pathway for Fe_3O_4 deposition [23]. Thus, a five minute deposition time was used in this study.

The morphology of the active material on the Cu nanorods is of great importance to achieve good rate capability. The ideal material should be composed of nano-sized, well crystallized particles that adhere firmly to the surface of the Cu nanorods to form dense and crack-free films. Our previous study showed that temperature plays a major role in determining the deposit morphology [19]. We found that capacity deteriorates quickly with loose Fe_3O_4 particles electrodeposited at low temperatures, i.e. 50 °C and have determined that 80 °C is suitable to obtain the desirable Fe_3O_4 deposits [19]. Fig. 1c–h shows the morphology of Fe_3O_4 deposited at 80 °C under the optimized conditions. It is clear in Fig. 1c and d, that after 1 min of electrodeposition, the Cu nanorods are uniformly covered with small Fe_3O_4 crystallites and their apparent diameters grow from 200 nm to 360 nm. A cross-sectional image shows that Fe_3O_4 crystallites deposited on the Cu nanorods are nanostructured and form a thin film on the Cu nanorods. This morphology ensures the intimate contact between Fe_3O_4 nanoparticles and the current collectors, which is crucial to gain the advantages of nanostructured electrodes, including shortened Li ion diffusion length during Li ion intercalation and good electric conductance between the current collectors and the active materials.

As shown in Fig. 1e, when the electrodeposition time of Fe_3O_4 is extended to 2 min, and after the Fe_3O_4 has filled all the inter-rod spaces between the Cu nanorods, it starts to form a continuous yet

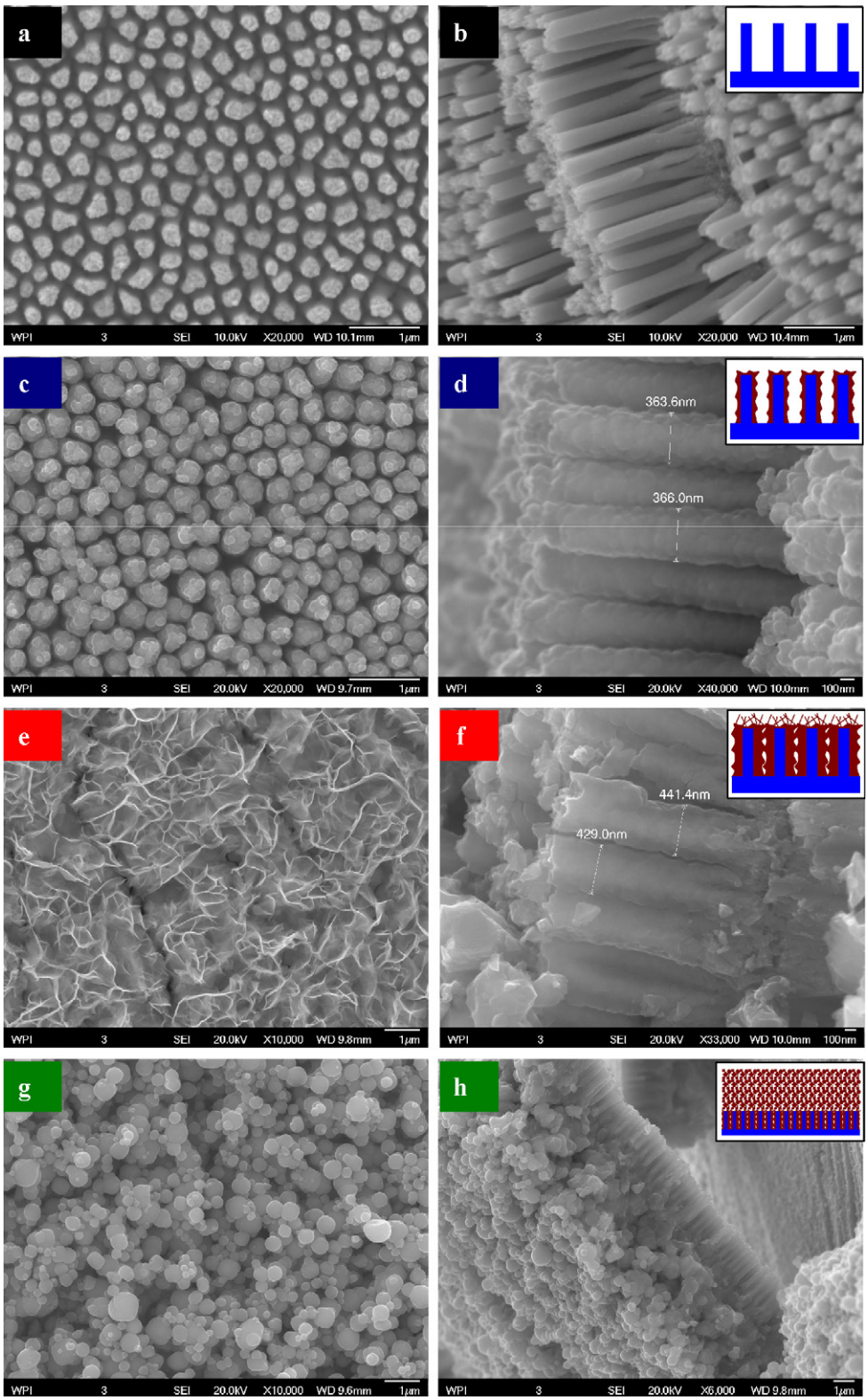

Fig. 1. SEM images of Cu nanorods before (a and b) and after Fe_3O_4 electrodeposition for (c and d) 1 min, (e and f) 2 min, and (g and h) 6 min. The insets show the cartoon of the Fe_3O_4 morphology with different deposition times.

porous film above the nanorod current collector array. The cross-sectional view in Fig. 1f further confirms that Fe_3O_4 crystallites between the Cu nanorods begin to coalesce into dense deposits on the surface of the nanorods as the electrodeposition lengthens. As a result, the apparent diameter of the nanorods increases to more than 420 nm. It is worth noting that these dense Fe_3O_4 deposits are undesirable for nanostructured electrodes because they may block the passage of electrolytes and Li ions, which subsequently can inhibit the advantages provided by Cu nanorod current collectors. When the electrodeposition time is increased to 6 min (Fig. 1g and h), Fe_3O_4 particles ranging from 100 to 1000 nm accumulate on top of the filled Cu nanorod arrays and form a 5-μm thick Fe_3O_4 film.

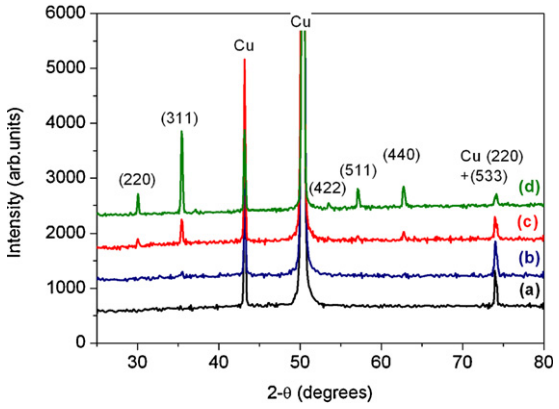

Fig. 2. XRD patterns of Fe_3O_4 electrodeposited at 80 °C and a current density of −5 mA cm^{-2} in solution 5 for (a) 0 min, (b) 1 min, (c) 2 min, and (d) 6 min.

During charge and discharge of the battery, the top micrometer-thick Fe_3O_4 film has direct exposure to the bulk electrolyte and there is less resistance for the Li ion transport compared with the Fe_3O_4 buried underneath this thick layer. As a result, the electrochemical reactions may preferably happen on the surface of the top micrometer-thick Fe_3O_4 film.

3.2. Microstructure study

Fig. 2 summarizes the typical X-ray diffraction (XRD) patterns of the as-prepared Fe_3O_4-based Cu nanostructured electrodes. The two strong peaks at 43.3° and 50.5° correspond to the plane (1 1 1) and the plane (2 0 0) reflections (International Centre for Diffraction Data card no. 04-0836) of the Cu substrate and the Cu nanorods. The Cu (2 0 0) reflection is much stronger than that of Cu (1 1 1), suggesting that the Cu substrate and the Cu nanorods are [1 0 0] textured. Fig. 2b indicates that the amount of Fe_3O_4 deposits after 60-s electrodeposition time is so little that the existence of the spinel Fe_3O_4 phase can hardly be detected. After 2 min electrodeposition time, the characteristic peaks for the spinel structure of Fe_3O_4 phase are recorded (Fig. 2c). The intensity of Fe_3O_4 diffraction peaks increases with increasing electrodeposition time. After 6 min electrodeposition (Fig. 2d), the iron oxide peaks match well with planes of Fe_3O_4 phase (ICDD card no. 19-0629), with the (3 1 1) reflection being the strongest. The strong and sharp Fe_3O_4 peaks suggest good crystallization of the as-deposited Fe_3O_4 under the present conditions. Comparison of the XRD patterns between the as-deposited Fe_3O_4 films and the randomly oriented powder sample suggests that the as-deposited Fe_3O_4 film has a random orientation.

3.3. Electrochemical performance

The charge/discharge performance and rate capability of the Fe_3O_4based Cu nanostructured electrodes with respect to Li were investigated. Electrochemical performance of Fe_3O_4 deposited on planar Cu disks under the same electrodepoistion conditions was recorded for comparison. The first two charge/discharge cycles were tested at a current rate of $C/10$ (8 lithium per Fe_3O_4 in 10 h), and the third and forth cycles at $C/5$. The corresponding discharge/charge voltage profiles are presented in Fig. 3. The shape of these profiles shows that Fe_3O_4 electrochemically reacts with Li via a conversion reaction process, which is consistent with previous reports [10,12,16,24]. There are two notable common features in all the electrodes during the first several cycles: (1) There is the characteristic electrochemical signature of the conversion reactions involved in transition-metal oxide during charge and discharge [1,12]. During discharge, the potential typically dropped rapidly

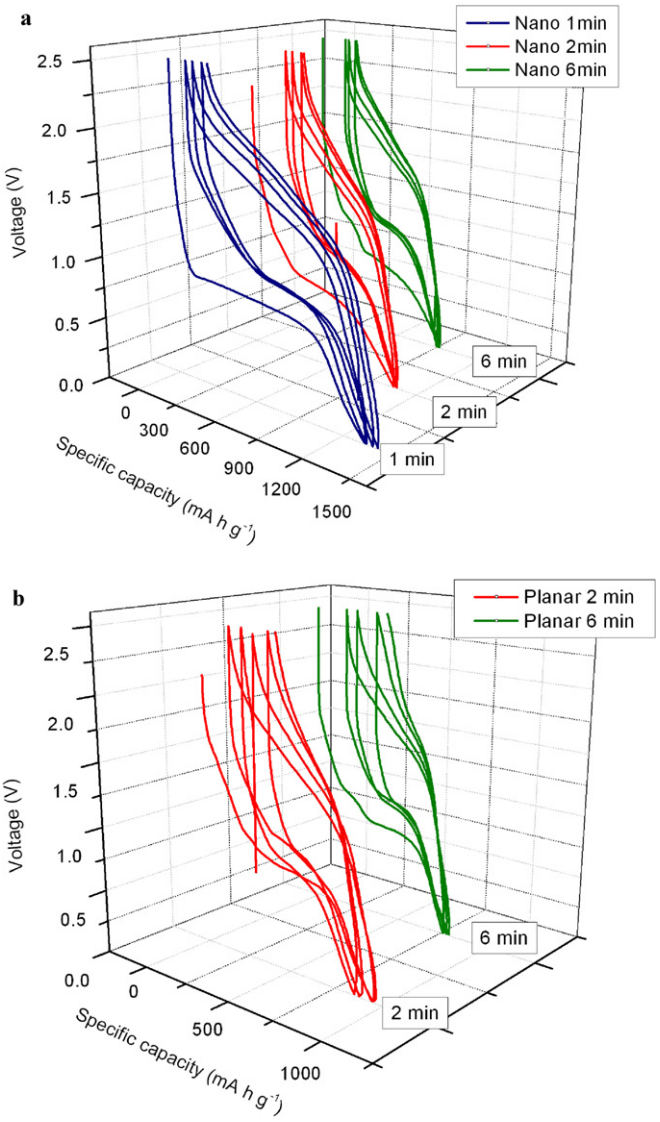

Fig. 3. The charge/discharge profiles of the as-prepared electrodes with different Fe_3O_4 deposition times: (a) 1, 2, and 6 min on Cu nanorod arrays; (b) 2 and 6 min on planar Cu disks. These cells were galvanostatically cycled versus Li at a rate of $C/10$ for the first two cycles and $C/5$ for the third and forth.

from 2.5 V to reach a well-defined plateau around 0.75 V. This corresponds to the full reduction of Fe_3O_4 into the Fe^0/Li_2O mixture, followed by additional capacity below 0.75 V where a gel-like film and solid electrolyte interphase (SEI) film form due to the reactions between the Fe_3O_4 particles and the electrolyte [25]. (2) The common charge/discharge hysteretic profiles which are inherent to conversion reactions are maintained.

Nevertheless, the difference between these profiles is of more interest. Fig. 3a, for example, presents the charge/discharge curves for the nanostructured electrode with 1 min Fe_3O_4 deposition time. The specific capacities of the first four discharges are 1342.23, 1220.69, 1208.68, and 1171.13 mAh g^{-1}, respectively, which, to our best knowledge, are the highest specific capacity values ever reported for the material of Fe_3O_4. It is notable that these capacity values are more than three times those of commercially used graphitic carbons (372 mAh g^{-1}). These specific capacities suggest 11.6, 10.6, 10.4, and 10.1 Li per Fe_3O_4 respectively can be reacted. Based on a complete reduction of Fe^{2+} and Fe^{3+} in Fe_3O_4 to Fe^0, one would expect a maximum uptake of 8 Li per Fe_3O_4. We attribute such high uptake of Li per Fe_3O_4 to the low-voltage decomposition

of the electrolyte and subsequent formation of an organic layer on the surface of the particles. Similar extra capacity was observed in other metal oxide systems such as nanostructured CuO [1], Fe_2O_3 [15,26], and CoO [27,28]. For conventional anode materials, the formation of SEI film is irreversible, leading to a one-time drop of capacity during the first charge/discharge cycle. For nanostructured oxide anode materials, interestingly, the extra capacity can be reversible. The reversible formation of a polymer/gel-like film was observed during charge/discharge cycling as a result of the electrolyte decomposition, accounting for the reversible extra capacity [28]. An interfacial lithium storage model was also employed to describe this extra capacity [29].

From Fig. 3a, the nanostructured electrodes with 2 and 6 min Fe_3O_4 deposition times show specific capacities of the first discharge to be 1046.65 and 922.40 mAh g^{-1} respectively, which is lower than that of a 1 min sample. This decrease, combined with the SEM images shown in Fig. 1, implies that the specific capacity is morphology-dependent. The active material of Fe_3O_4 in the electrode with 1 min Fe_3O_4 deposition time has better coverage on each Cu nanorod without coalescence and thus has a larger specific surface area compared to those with longer deposition times. The larger specific surface area provides more reaction area and is favorable for SEI film formation during charge/discharge. This ultimately leads to higher specific capacity.

To further prove this point, the charge/discharge profiles of Fe_3O_4 deposited for 2 and 6 min on planar Cu substrates are shown in Fig. 3b. Their morphology has been reported elsewhere [19]. Briefly, the Fe_3O_4 deposits after 2 min deposition time have a continuous and porous morphology, and consist of a mixture of Fe_3O_4 flakes and particles. Contrastingly, the Fe_3O_4 deposits after 6 min deposition time are composed of densely packed Fe_3O_4 particles sizes ranging from 100 to 1000 nm, similar to the morphology of the top layer shown in Fig. 1g. Fig. 3b shows that the specific capacities of the first discharge are 964.75 and 795.27 mAh g^{-1} for 2 min and 6 min deposition time, respectively. These results again emphasize the importance of using Cu nanorod arrays as the current collector and maintaining an open morphology in Fe_3O_4 deposits. It is important to have an unobstructed and easy pathway for Li ions to transport to obtain a high specific charge/discharge capacity.

The capacity retention of the nanostructured electrodes as well as the planar counterparts was tested with the coin cells cycled galvanostatically between 2.5 and 0.02 V versus Li^+/Li^0 at different rates. For the data shown in Fig. 4, the cells were cycled at rates of *C*/10, *C*/5, and *C*/2 for cycles 1–2, cycles 3–5, and cycles 6–9, respectively and the schedule repeated in the following cycles. The plots in Fig. 4 show a common trend that the specific capacity decreases with the increasing current rate [12,14,15]. However, the nanostructured electrodes possess a much better capacity retention compared to the planar ones. The nanostructured electrodes with 2 and 6 min Fe_3O_4 deposition time exhibit specific discharge capacities of 460.88 and 354.65 mAh g^{-1} after 50 cycles, corresponding to 44.03% and 38.45% of their initial capacities. Contrastingly, the discharge capacities of the planar electrodes drop drastically after 10 cycles. The planar electrodes manifest capacities of 153.90 and 97.90 mAh g^{-1} after 50 cycles, corresponding to 12.31% 15.86% of their initial capacities. Another remarkable observation from Fig. 4 is that the nanostructured electrode with 1 min Fe_3O_4 deposition time shows a very high sustained reversible capacity and good rate capability. The specific discharge capacity in cycle 32 is 922.10 mAh g^{-1} at a rate of *C*/2 and that after 34 cycles is 1003.94 mAh g^{-1} at a rate of *C*/10 which counts for 74.80% of the initial discharge capacity. This dramatic difference is probably due to, other than the different particle sizes of the deposited Fe_3O_4, the fact that the Cu nanorod arrays provide a robust mechanical support to Fe_3O_4 deposits. The support can accommodate the

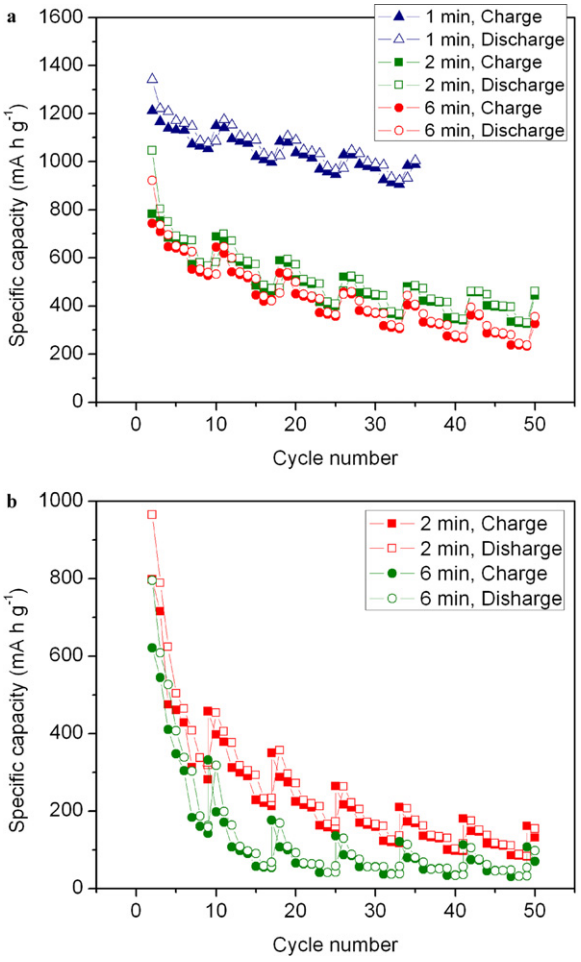

Fig. 4. The capacity retention of Fe_3O_4 film electrodeposited onto (a) nanostructured and (b) planar copper substrates for different times and cycled at rates of *C*/10, *C*/5, and *C*/2.

structure strains and retain the openness of the structure during Li ion insertion and extraction [12,16]. The post-cycling examination of the electrodes by optical microscopy shows that some Fe_3O_4 deposits on the planar electrodes and nanostructured electrodes with long deposition times (>2 min) peeled off from the Cu collector; the nanostructured electrode with 1 min Fe_3O_4 deposition time, in contrast, looked solid and clean. SEM observation shows that for the electrode with 1 min Fe_3O_4 deposition, the intimate contact between Fe_3O_4 nanoparticles and the current collectors is retained. This reemphasizes the importance of the morphology of the as-prepared nanostructured electrode to achieve the structure stability during cycling.

Finally, the comparison between the nanostructured Fe_3O_4 electrode and the commercially used graphitic carbon readily shows that the Fe_3O_4 electrode based on the "conversion reactions" provides much larger specific capacity. Moreover, good capacity retention and rate capability can be achieved by tailoring the morphology of the Fe_3O_4 deposits. Considering the difference in density (2.23 g cm^{-3} for graphite and about 5.1 g cm^{-3} for Fe_3O_4), the advantage of Fe_3O_4-based electrodes in the volumetric specific capacity is even more significant. However, the hysteresis in the charge/discharge profiles must be considerably reduced or the cell polarization must be decreased before the conversion-reaction-based electrodes are considered to replace graphite. Plus, the intrinsic limitation of this architecture might be the limit on the aspect-ratio of the Cu nanorods to avoid aggregation. This limits the amount of the active material that can be accommo-

dated between the nanorods and thus makes scaling-up of the architecture for commercial applications difficult no matter what active material is chosen. Therefore, we need to balance the benefit of having Cu nanorods to obtain maximum capacity of active material and the increase in the weight of the electrode with subsequent decrease in relative amount of the active material due to the existence of Cu nanorods. On the one hand, sufficient amount of Cu nanorods is needed to provide large surface for Fe_3O_4 deposition, which will unfortunately decrease the overall energy density. On the other hand, the aspect-ratio is limited to avoid aggregation. We also want to point out that the aspect-ratio limit is related to the size, spacing, and density of the Cu nanorods. In this report we employed AAO templates to assist in Cu nanorod deposition. In the follow-up studies, lithographical approaches might be more suitable to provide accurately defined size and spacing of Cu nanorods to determine the optimal size, spacing and density of the Cu nanorods for maximizing the overall energy density of the anode. However, our study confirms that three-dimensional nanostructured electrode design can take better advantage of active materials following conversion reaction mechanism. And our report identified a few key issues, such as the need to maintain a thin film of active material with intimate and uniform contact with current collectors on the nanoscale. Therefore, further research may include seeking active materials with less cell polarization, and improving or inventing other design of 3D nanostructured electrodes employing new classes of active materials. Moreover, the design of thin film lithium ion battery incorporating 3D nanostructured anode can be explored for energy storage in situations where extremely high energy density and power density are required.

4. Conclusions

The Fe_3O_4-based Cu nanostructured electrodes for Li ion batteries were fabricated by a two-step electrochemical process. SEM images show that after 1 min Fe_3O_4 deposition time, the Cu nanorods were uniformly covered with a dense layer of nano-sized Fe_3O_4 crystallites. The electrochemical performance is closely related to the deposition time in current experiments, with the nanostructured electrodes with 1 min Fe_3O_4 deposition exhibiting the largest specific discharge capacity. Long electroplating time leads to the filling of the spaces between the Cu nanorods in addition to the coalescence of Fe_3O_4 particles on the top of the Cu nanorod arrays. This causes difficulty when achieving high specific sustained reversible capacities and good rate capability.

Acknowledgements

The financial support for this work from NASA (contract no. NNJ07JB33C) and OSD/ONR (contract nos. N00014-07-M-0110 and 07PR06126-00) are gratefully acknowledged. Huanan Duan would like to thank Meghan Pasquali for her proofreading.

References

[1] P. Poizot, S. Laruelle, S. Grugeon, L. Dupont, J.M. Tarascon, Nature 407 (2000) 496–499.
[2] N. Li, C.R. Martin, B. Scrosati, J. Power Sources 97–98 (2001) 240–243.
[3] X. He, W. Pu, L. Wang, J. Ren, C. Jiang, C. Wan, Electrochim. Acta 11 (2007) 3651–3653.
[4] V. Subramanian, A. Karki, K.I. Gnanasekar, F. Eddy, B. Rambabu, J. Power Sources 159 (2006) 186–192.
[5] H. Wang, T. Abe, S. Maruyama, Y. Iriyama, Z. Ogumi, K. Yoshikawa, Adv. Mater. 17 (2005) 2857–2860.
[6] M. Park, Y. Kang, G. Wang, S. Dou, H. Liu, Adv. Funct. Mater. 18 (2008) 455–461.
[7] E. Hosono, S. Fujihara, I. Honma, M. Ichihara, H. Zhou, J. Electrochem. Soc. 153 (2006) A1273–A1278.
[8] A.S. Arico, P. Bruce, B. Scrosati, J.M. Tarascon, W.V. Schalkwijk, Nat. Mater. 4 (2005) 366–377.
[9] C.R. Sides, N. Li, C.J. Patrissi, B. Scrosati, C.R. Martin, MRS Bull. 26 (2002) 604–608.
[10] S. Mitra, P. Poizot, A. Finke, J.M. Tarascon, Adv. Funct. Mater. 16 (2006) 2281–2287.
[11] S. Ito, K. Nakaoka, M. Kawamura, K. Ui, K. Fujimoto, N. Koura, J. Power Sources 146 (2005) 319–322.
[12] P.L. Taberna, S. Mitra, P. Poizot, J.M. Tarascon, Nat. Mater. 5 (2006) 567–573.
[13] D. Larcher, C. Masquelier, D. Bonnin, Y. Chabre, V. Masson, J.B. Leriche, J.M. Tarascon, J. Electrochem. Soc. 150 (2003) A133–A139.
[14] W.M. Zhang, X.L. Wu, J.S. Hu, Y.G. Guo, L.J. Wan, Adv. Funct. Mater. 18 (2008) 3941–3946.
[15] F. Jiao, J. Bao, P.G. Bruce, Electrochem. Solid-State Lett. 10 (2007) A264–A266.
[16] H. Duan, J. Gnanaraj, X. Chen, B. Li, J. Liang, J. Power Sources 185 (2008) 512–518.
[17] L. Bazin, S. Mitra, P.L. Taberna, P. Poizot, M. Gressier, M.J. Menu, A. Barnabe, P. Simon, J.M. Tarascon, J. Power Sources 188 (2009) 578–582.
[18] X.H. Huang, J.P. Tu, X.H. Xia, X.L. Wang, J.Y. Xiang, L. Zhang, Y. Zhou, J. Power Sources 188 (2009) 588–591.
[19] H. Duan, X. Chen, B. Li, J. Liang, Mater. Res. Bull. 45 (2010) 1696–1702.
[20] H.M. Kothari, E.A. Kulp, S.J. Limmer, P. Poizot, E.W. Bohannan, J.A. Switzer, J. Mater. Res. 21 (2006) 293–301.
[21] H. Chik, J. Liang, S.G. Cloutier, N. Koukli, J.M. Xu, Appl. Phys. Lett. 84 (2004) 3376–3378.
[22] J. Liang, H. Chik, J. Xu, IEEE J. Sel. Top. Quantum Electron. 8 (2002) 998–1008.
[23] X. Chen, H. Duan, Z. Zhou, J. Liang, J. Gnanaraj, Nanotechnology 19 (2008) 365306.
[24] A. Finke, P. Poizot, C. Guery, D. Razouzi, J.M. Tarascon, Adv. Funct. Mater. 18 (2008) 3598–3605.
[25] S. Wang, J. Zhang, C. Chen, J. Power Sources 195 (2010) 5379–5381.
[26] L. Wang, H.W. Xu, P.C. Chen, D.W. Zhang, C.X. Ding, C.H. Chen, J. Power Sources 193 (2009) 846–850.
[27] P. Poizot, S. Laruelle, S. Grugeon, L. Dupont, B. Beaudoin, J.M. Tarascon, Ann. Isr. Phys. Soc. 3 (2000) 681–691.
[28] S. Grugeon, S. Laruelle, L. Dupont, J.M. Tarascon, Solid State Sci. 5 (2003) 895–904.
[29] J. Jamnik, J. Maier, Phys. Chem. Chem. Phys. 5 (2003) 5215–5220.